Molecular and Cellular Endocrinology 351 (2012) 317–325

Contents lists available at SciVerse ScienceDirect

Molecular and Cellular Endocrinology

journal homepage: www.elsevier.com/locate/mce

Nanomolar dose of bisphenol A rapidly modulates spinogenesis in adult hippocampal neurons

Nobuaki Tanabe [a,1], Hinako Yoshino [a,1], Tetsuya Kimoto [a,c], Yasushi Hojo [a,c,d], Mari Ogiue-Ikeda [a,b], Yasuyuki Shimohigashi [e], Suguru Kawato [a,b,c,d,*]

[a] Department of Biophysics and Life Sciences, Graduate School of Arts and Sciences, The University of Tokyo, Komaba 3-8-1, Meguro, Tokyo 153-8902, Japan
[b] National MEXT Project in Special Coordinate Funds for Promoting Science and Technology, The University of Tokyo, Japan
[c] Core Research for Evolutional Science and Technology Project of Japan Science and Technology Agency, The University of Tokyo, Japan
[d] Bioinformatics Project, Japan Science and Technology Agency, The University of Tokyo, Japan
[e] Department of Chemistry, Faculty and Graduate School of Sciences, Kyushu University, Hakozaki 6-10-1, Higashi, Fukuoka 812, Japan

ARTICLE INFO

Article history:
Received 6 July 2011
Received in revised form 23 November 2011
Accepted 9 January 2012
Available online 16 January 2012

Keywords:
Bisphenol A
Endocrine disrupter
ERRγ
Hippocampus
Spine
Estradiol

ABSTRACT

We demonstrated the rapid effects of 10 nM bisphenol A (BPA) on the spinogenesis of adult rat hippocampal slices. The density of spines was analyzed by imaging Lucifer Yellow-injected CA1 neurons in slices. Not only the total spine density but also the head diameter distribution of spine was quantitatively analyzed. Spinogenesis was significantly enhanced by BPA within 2 h. In particular, the density of middle-head spine (with head diameter of 0.4–0.5 μm) was significantly increased.

Hydroxytamoxifen, an antagonist of both estrogen-related receptor gamma (ERRγ) and estrogen receptors (ERα/ERβ), blocked the BPA-induced enhancement of the spine density. However, ICI 182,780, an antagonist of ERα/ERβ, did not suppress the BPA effects. Therefore, ERRγ is deduced to be a high affinity receptor of BPA, responsible for modulation of spinogenesis. The BPA-induced enhancement of spinogenesis was also suppressed by MAP kinase inhibitor, PD98059, and the blocker of NMDA receptors, MK-801. Washout of BPA for additional 2 h after 2 h BPA treatment abolished the BPA-induced enhancement of spinogenesis, suggesting that the BPA effect was reversible. ERRγ was localized at synapses as well as cell bodies of principal neurons. ERRγ at synapses may contribute to the observed rapid effect. The level of BPA in the hippocampal slices was determined by mass-spectrometric analysis.

1. Introduction

Low dose exposure to bisphenol A (BPA) may induce hormone-like effects on wildlife and humans. BPA is a widely used synthetic material included in polycarbonate resin used in water pipe sealant, dental prostheses, compact discs and baby bottles. Toxic effects of high dose BPA (mg/kg weight/day) have been investigated in relation to the development and functions of the reproduction systems (Fisher et al., 1999; Al-Hiyasat et al., 2002; Grote et al., 2004; Halldin et al., 2005). However, the low dose exposure to BPA (μg/kg/day or nanomolar doses) shows rather weak toxic effects on reproductive or endocrine functions in the peripheral tissues, probably due to the efficient detoxification of BPA by the liver. On the other hand, low dose exposure to BPA may significantly affect the brain function, because the detoxification of BPA in the brain is probably very weak, due to the extremely low expression of drug-metabolizing enzymes in the brain (Miksys and Tyndale, 2002; Kishimoto et al., 2004; Chinta et al., 2005).

The low dose exposure to BPA during fetal/neonatal stages has been extensively investigated. For example, fetal or neonatal exposure to BPA inhibits sexual differentiation of nonreproductive behaviors of adult animals, including maze learning behavior (Carr et al., 2003; Kubo et al., 2003; Fujimoto et al., 2006), at doses as low as 1/1000 of those required for the stimulation of uterine growth (Ashby, 2001). On the other hand, inadequate information is available for the low dose exposure to BPA in the adult stage, except some pioneer works *in vivo* (MacLusky et al., 2005; Leranth et al., 2008; Hajszan and Leranth, 2010).

The high affinity functional receptor for BPA has not been identified yet. Although ERα is one candidate of BPA receptor, the

Abbreviations: ACSF, artificial cerebrospinal fluid; AMPA, α-amino-3-hydroxy-5-methyl-4-isoxazolepropionic acid; BPA, bisphenol A; CNQX, 6-cyano-7-nitroquinoxaline-2,3-dione; DG, dentate gyrus; E2, 17β-estradiol; ER, estrogen receptor; ERRγ, estrogen-related receptor gamma; ICI, ICI182,780; MR, median raphe; MSDB, medial septum/diagonal band of Broca; NMDA, *N*-methyl-D-aspartate; OH-Tam, 4-hydroxytamoxifen; OVX, ovariectomized; PSD, postsynaptic density; PY, pyramidal neurons; SUM, supramammillary area.

* Corresponding author at: Department of Biophysics and Life Sciences, Graduate School of Arts and Sciences, The University of Tokyo, Komaba 3-8-1, Meguro, Tokyo 153-8902, Japan. Tel./fax: +81 3 5454 6517.
E-mail addresses: kawato@phys.c.u-tokyo.ac.jp, kawato@bio.c.u-tokyo.ac.jp (S. Kawato).

[1] These authors contributed equally.

0303-7207/$ - see front matter © 2012 Elsevier Ireland Ltd. All rights reserved.
doi:10.1016/j.mce.2012.01.008

affinity of ERα for BPA is very low, in the order of 1/100–1/1000 of that for 17β-estradiol (E2) (Kuiper et al., 1997; Morohoshi et al., 2005). On the other hand, estrogen-related receptor gamma (ERRγ) is a high affinity binding protein for BPA (Takayanagi et al., 2006). However, ERRγ has not been recognized as a BPA receptor, because ERRγ shows constitutive transcriptional activity even without any ligand (Coward et al., 2001).

We here performed the investigation on the rapid modulation by nanomolar doses of BPA on the density and morphology of dendritic spines in the adult hippocampal slices, including investigations of BPA receptors. In order to observe the direct effects of BPA on hippocampal neurons, we used isolated 'acute' hippocampal slices which do not have projections of cholinergic or serotonergic neurons from outside of the hippocampus.

2. Materials and methods

2.1. Chemicals

BPA, 6-cyano-7-nitroquinoxaline-2,3-dione (CNQX), cycloheximide, nicardipine, *N*-methyl-D-aspartate (NMDA), PD98059, ICI 182,780 (ICI), MK-801 and Lucifer Yellow were purchased from Sigma (USA). 4-hydroxy-tamoxifen (OH-Tam) was from Calbiochem (Germany). Other chemicals used were of highest purity commercially available. Polyclonal anti-ERRγ antibody (against C-terminal of ligand binding site) was prepared by Dr. Shimohigashi at Kyushu Univ. (Tokunaga et al., 2006).

2.2. Animals

Adult male Wistar rats (12 weeks old, 340–360 g) were purchased from Saitama Experimental Animal Supply (Saitama, Japan). The experimental procedure of this research was approved by the Committee for Animal Research of the University of Tokyo.

2.3. Preparation of 'acute' hippocampal slices

Rats were deeply anesthetized with ethyl ether and decapitated. The brains from adult rats were removed and placed at 4 °C in artificial cerebrospinal fluid (ACSF) consisted of (mM): 124 NaCl, 5.0 KCl, 1.25 NaH_2PO_4, 2.0 $MgSO_4$, 2.0 $CaCl_2$, 22 $NaHCO_3$, 10 glucose and was equilibrated with 95% O_2/5% CO_2. The hippocampus was dissected and 300 μm-thick transverse dorsal 'fresh' slices to the long axis were prepared with a vibratome (Dosaka EM, Kyoto, Japan). 'Acute' slices were prepared from these 'freshly prepared' slices by 2 h recovery incubation at 25 °C in ACSF.

2.4. Imaging and analysis of spinogenesis

Experimental details are described in elsewhere (Mukai et al., 2007).

2.4.1. Current injection of Lucifer Yellow

'Acute' slices were further incubated with BPA in the presence or absence of other drugs such as OH-Tam or PD98059. Drug-treated slices were then prefixed with 4% paraformaldehyde in PBS (0.1 M phosphate buffer and 0.14 M NaCl, pH 7.3) at 4 °C for 2–4 h.

Neurons within slices were visualized by an injection of Lucifer Yellow under a Nikon E600FN microscope (Japan) equipped with a C2400–79H infrared camera (Hamamatsu Photonics, Japan) and with a 40× water immersion lens (Nikon). A glass electrode was filled with 5% Lucifer Yellow, which was then injected for 15 min using Axopatch 200B (Axon Instruments, USA). Approximately five neurons within a 100–200 μm depth from the surface of a slice were injected (Duan et al., 2002). After injection, slices were fixed again with 4% paraformaldehyde at 4 °C overnight.

2.4.2. Confocal laser microscopy and morphological analysis

The imaging was performed from sequential *z*-series scans with LSM5 PASCAL confocal microscope (Zeiss, Germany). For analysis of spines, three-dimensional images were constructed from approximately 40 sequential *z*-series sections of neurons scanned every 0.45 μm with a 63× water immersion lens, NA 1.2 (Zeiss). For Lucifer Yellow, the excitation and emission wavelengths were 488 nm and 515 nm, respectively. The applied zoom factor (3.0) yielded 23 pixels per 1 μm. The *z*-axis resolution was approximately 0.71 μm. The confocal lateral resolution was approximately 0.26 μm. Confocal images were then deconvoluted using AUTODEBLUR software (AutoQuant, USA). The density of spine as well as the head diameter was analyzed with Spiso-3D (automated software mathematically calculating geometrical parameters of spines) developed by Bioinformatics Project of Kawato's group (Mukai et al., 2011). Results obtained by Spiso-3D are almost identical to those by Neurolucida (manual-based analysis software) (MicroBrightField, USA) within assessment difference of 2%, and Spiso-3D considerably reduces human errors and experimental labor of manual software. We analyzed the secondary dendrites in the stratum radiatum, lying between 100 and 250 μm from the soma. The spine density was calculated from the number of spines on dendrites having a total length of 50–80 μm. In total, we investigated 3–4 rats, 6–8 slices, 12–16 neurons, 24–32 dendrites and 1200–2000 spines. Spine shapes were classified into three categories as follows. (1) A small-head spine whose head diameter is 0.2–0.4 μm. (2) A middle-head spine whose head diameter is 0.4–0.5 μm. (3) A large-head spine whose head diameter is 0.5–1.0 μm. These three categories were useful to distinguish different responses upon inhibitor application. Because the majority of spines (>95%) had a distinct head and neck, and stubby type and filopodium type spines did not contribute much to overall changes, we analyzed spines having a distinct head.

All protrusions from the dendrites were treated as 'spines', although with confocal microscopy, it was not possible to determine whether they formed synapses, or whether some of them were filopodia protrusions which did not form synapses (Sorra and Harris, 2000). While counting the spines in the reconstructed images, the position and verification of spines were aided by rotation of three-dimensional reconstructions and by observation of the images in consecutive single planes.

2.5. Immunohistochemical staining of hippocampal slices

Immunohistochemical staining of hippocampal slices was performed as described in elsewhere (Kimoto et al., 2001; Kawato et al., 2002) and Supplementary material. Staining of ERRγ was performed using the avidin–biotin peroxidase complex technique. After application of anti-ERRγ antibody (1/250), the slices were incubated for 24 h at 4 °C, in the presence of 0.5% Triton X-100 and 3% skim milk with gentle shaking.

For preabsorption of anti-ERRγ antibody with antigen, excess amount of antigen was preincubated with anti-ERRγ antibody for 15 h at 4 °C. Characterization of anti-ERRγ antibody is described in Supplementary material with Fig. S1.

2.6. Preparation of synaptic, cytoplasmic and nuclear fractions

Fractionation of the homogenates obtained from hippocampal slices was performed by a combination of centrifugations at 4 °C (Cohen et al., 1977). Detailed procedures to obtain the raft fraction, nuclear fraction, postsynaptic density (PSD) fraction, low density membrane fraction (presynaptic membrane-enriched fraction),

high density membrane fraction (microsome and postsynaptic membrane-enriched fraction), and the cytoplasmic fraction are described in elsewhere (Mukai et al., 2007) and Supplementary material.

2.7. Western immunoblot analysis

The protein blots were probed with anti-ERRγ antibody (diluted to 1/3000) for 12 h at 4 °C, and incubated with horseradish peroxidase-conjugated goat anti-rabbit IgG. Detailed procedures are described in Supplementary material.

2.8. Mass-spectrometric assay of BPA

Experimental details are described in elsewhere (Hojo et al., 2009) and Supplementary material. The extraction of steroids from hippocampal slices was performed by hexane: ethylacetate = 2:3 mixtures. The steroid extracts were applied to a C_{18} Amprep solid phase column (Amersham Biosciences, Piscataway, NJ). The BPA fraction was separated from eluted steroids using a normal phase HPLC system (Jasco, Tokyo, Japan) with a silica gel column. The recoveries of BPA through the steps above were approx 40%. To increase the ionization efficiency, BPA was derivatized to BPA-dipicolinoyl-ester (Hojo et al., 2009). The LC–MS/MS system, which consisted of a reverse phase LC coupled with an API 5000 triple-stage quadrupole mass spectrometer (Applied Biosystems, Foster City, CA), was operated with electron spray ionization. The LC chromatographic separation for BPA derivatives was performed on Cadenza CD-C_{18} column (Imtakt, Kyoto, Japan). The MS/MS process monitored the m/z transition from 439.3 to 239.8 Deuterium labeled BPA derivative (2, 2′, 6, 6′-d_4-BPA-dipicolinoyl-ester) was used for internal standards in order to measure the recovery of BPA as well as to calibrate the retention time. After derivatization, purification and MS/MS detection, the recovery for BPA was determined to be approximately 70%. The limit of quantification for BPA was 5 pg per 0.1 g of hippocampal tissue (Table S1). The linearity was observed between 5 pg and 1000 pg. For more detailed procedures, see Supplementary material.

2.9. Statistical analysis

In spine analysis, data are expressed as mean ± SEM. The significance of drug effect was examined via statistical analysis using Tukey–Kramer post hoc multiple comparison test when one way ANOVA tests yielded $P < 0.05$.

3. Results

3.1. Rapid effect of BPA on spinogenesis

We analyzed the effect of BPA on the modulation of the density and head diameter of spines in the CA1 region. To do this, single spine imaging was performed for Lucifer Yellow-injected neurons in hippocampal slices from adult male rats. We analyzed secondary branches of the apical dendrites located 100–200 μm distant from the pyramidal cell body around the middle of the stratum radiatum of CA1 region.

3.1.1. Total spine density analysis

Following a 2 h treatment with BPA, dendrites had significantly more spines than control (Fig. 1–1). Time dependency was examined by treating slices for 0, 0.5, 1, 1.5 and 2 h with 10 nM BPA. The enhancing effect on the total spine density was approximately proportional to the incubation time, showing 0.94 (0 h), 0.95 (0.5 h), 1.21 (1 h), 1.21 (1.5 h) and 1.58 spines/μm (2 h) (Figs. 1 and 2). Dose dependency was also examined after 2 h incubation. Dose dependency showed that the enhancing effect was most significant at 10 nM BPA (1.55 spines/μm) as compared with 1 nM (0.95 spines/μm), 100 nM (1.40 spines/μm) and 10 μM BPA (0.92 spines/μm) (Figs. 1 and 2). Because a 2 h treatment with 10 nM BPA was most effective in spinogenesis, this incubation condition was used in the following investigations unless specified.

To investigate signaling pathway of BPA-induced increase in the total spine density, several antagonists and blockers were applied (Fig. 2).

Application of ICI, an antagonist of ERα/ERβ, did not suppress the increase in the spine density by 10 nM BPA (1.56 spines/μm). On the other hand, application of OH-Tam, an antagonist of both ERRγ and ERα/ERβ, completely suppressed the enhancement of spine density by BPA (0.94 spines/μm).

Application of MK-801, an antagonist of NMDA receptor, completely suppressed the enhancement of spine density by BPA (0.96 spines/μm). Application of CNQX, an antagonist of AMPA receptor, partially-prevented the enhancement by BPA (1.24 spines/μm). Application of nicardipine, an antagonist of L-type voltage-dependent Ca^{2+} channel, did not inhibit the enhancement of spine density induced by 10 nM BPA (1.48 spines/μm). When Ca^{2+} free ACSF was used, BPA-induced spinogenesis was completely suppressed (0.80 spines/μm). Application of PD98059, an inhibitor of Erk MAP kinase, completely prevented the BPA-induced spinogenesis (0.84 spines/μm). Washout of BPA for additional 2 h after the 2 h BPA treatment abolished the BPA-induced enhancement of spinogenesis, implying that the BPA effect was reversible. It should be noted that inhibitors (OH-Tam, ICI, PD98059) alone did not significantly affect the total spine density within experimental error, indicating that the observed inhibitory effects are not due to simple blocker's poison effects (Fig. S2 in Supplementary material).

3.1.2. Spine head diameter analysis

The morphological changes in the spine head diameter induced by a 2 h treatment with 10 nM BPA were assessed (Fig. 3). The majority of spines (>95%) had a distinct head, therefore we statistically analyzed these spines having distinct heads. We classified the spines into three categories depending on their head diameter, i.e. small-head spines (0.2–0.4 μm), middle-head spines (0.4–0.5 μm), and large-head spines (0.5–1.0 μm). The categorization into three subclasses enabled to distinguish different responses in spine subpopulations upon application of BPA, receptor antagonist or kinase inhibitor. Small-, middle-, and large-head spines are different in the density of AMPA receptors (Shinohara et al., 2008), therefore these three types of spines may have different physiological functions. The density of AMPA receptors in the spine positively correlates with the postsynaptic density (PSD) area size.

We performed a statistical analysis using three subclasses (Fig. 3B). In control slices (0 nM BPA), the spine density was 0.14 spines/μm for small-head spines, 0.40 spines/μm for middle-head spines, and 0.45 spines/μm for large-head spines. Upon treatment with BPA, the density of middle-head spines increased significantly to 0.60 spines/μm, while the density of small-head and large-head spines was not significantly altered (Fig. 3B). The co-application of OH-Tam with BPA considerably suppressed BPA-induced increase in the density of middle-head spines to 0.35 spines/μm (Fig. 3B). No significant change in BPA-induced increase in the density of three subclasses of spines was induced by co-application with ICI (Fig. 3B).

3.2. Staining of ERRγ

Hippocampal distribution of ERRγ was investigated by immunostaining of hippocampal slices with anti-ERRγ antibody. A strong immunostaining of pyramidal and granule neurons was observed in CA1–CA3 and DG (Fig. 4–1). No staining was observed

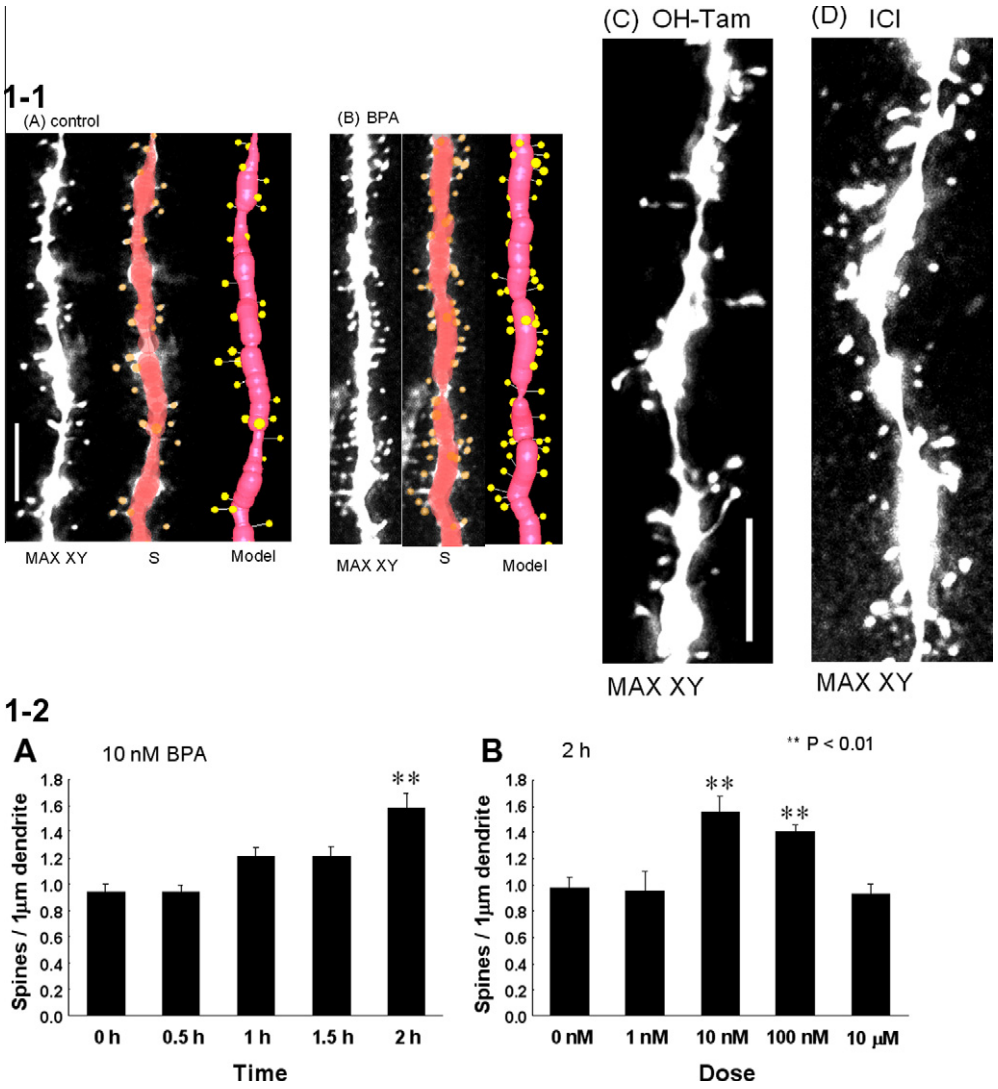

Fig. 1. Effect of BPA on spines in adult hippocampal CA1 neurons (1-1) Spine images along the secondary dendrites in the stratum radiatum. Maximal intensity projections onto XY plane from *z*-series confocal micrographs (Max XY), spine images analyzed by Spiso-3D (S) and 3 dimensional model illustration (Model). (A) Control spines without drug-treatments (control, 0 nM BPA), (B) with 10 nM BPA (BPA), and (C) with 10 nM BPA and 1 μM OH-Tam (OH-Tam), and (D) with 10 nM BPA and 1 μM ICI (ICI). Bar = 5 μm. (1-2) (A) Time-dependence of BPA effect. The total spine density after 0, 0.5, 1, 1.5 and 2 h treatments with 10 nM BPA. Vertical axis is the total number of spines per 1 μm dendritic segment. Results are reported as means ± SEM. Statistical significance, $^{**}P < 0.01$ vs. control (0 h). (B) Dose-dependence of BPA effect on total spine density. Vertical axis is the total spine density after a 2 h treatment with 0 nM, 1 nM, 10 nM, 100 nM and 10 μM of BPA. Statistical significance, $^{**}P < 0.01$ vs. control (0 nM BPA). For each condition, we investigated 3–4 rats, 6–8 slices, 12–16 neurons, 24–32 dendrites and 1200–2000 spines.

when anti-ERRγ antibody preabsorbed with the excess amount of antigen peptide was used as a primary antibody. Subcellular expression of ERRγ was analyzed by Western blot. A clear single band with M.W. of approx. 55 kDa was observed in PSD fraction, dendritic raft fraction and nuclear fraction of hippocampal neurons (Fig. 4–2).

3.3. Concentration of BPA in the hippocampus

Because BPA is widely present in environments, the endogenous concentration of BPA was carefully determined for adult male rat hippocampus with mass-spectrometric investigations using a chromatogram analysis of the fragmented ions (Fig. 5–1). After selection of mother ions, fragmentation and detection were performed via MS/MS procedures. Chromatographic profiles for the fragmented ions of BPA-dipicolinoyl-ester having $m/z = 239.8$ showed a clear peak with the retention time of 5.18 min which was the same as that of the standard BPA derivative (Fig. 5–1). The average concentration of BPA in 'fresh' hippocampal slices (before incubation with ACSF) was evaluated to be 14.6 ± 1.8 ng/g wet weight (i.e., 64 ± 8 nM) from 4 animals. In contrast, the BPA concentration in 'acute' slices, used for spinogenesis experiments, was less than 0.5 nM, due to significant release of BPA to ACSF during 2 h recovery incubation (Fig. 5–2). These results imply that the elevation of BPA from <0.5 nM to 10 nM occurred upon application of 10 nM BPA in acute slices in spinogenesis experiments.

We need to subtract blank values of BPA (0.027 ± 0.006 ng/mL) that was measured in blank samples which were prepared alongside hippocampal samples through the whole extraction, fractionation and purification procedures. These subtraction procedures are essential, because BPA was observed even in pure water (see Supplementary material).

4. Discussion

Current investigations of the rapid effects of BPA on spinogenesis in isolated hippocampal slices lead to the finding of ERRγ-mediated BPA action at synapses of pyramidal neurons.

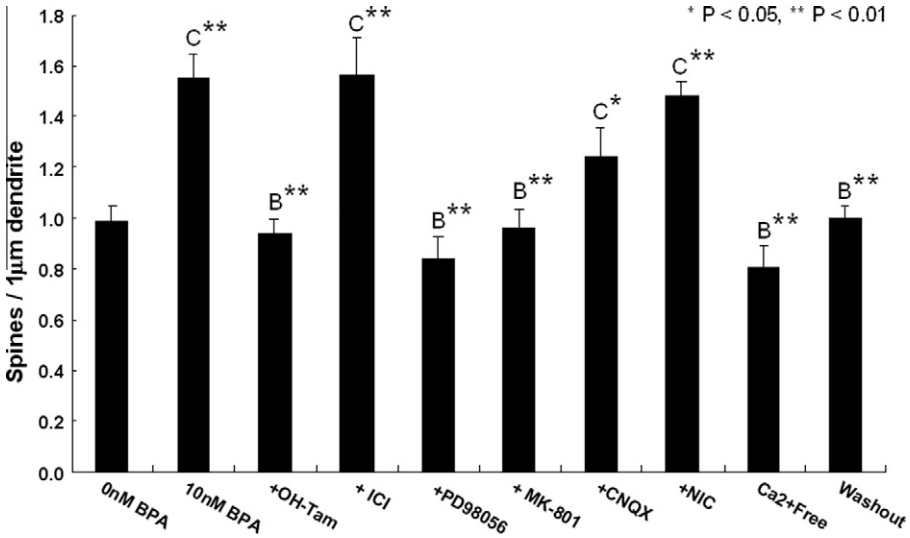

Fig. 2. Total spine density analysis for treatments with BPA, blockers of receptors and inhibitor of kinase. A 2 h treatment in ACSF without BPA (0 nM BPA), with 10 nM BPA (10 nM BPA), with 10 nM BPA and 1 μM OH-Tam (+OH-Tam), with 10 nM BPA and 1 μM ICI (+ICI), with 10 nM BPA and 50 μM 29 PD98059 (+ PD98059), with 10 nM BPA and 20 μM MK-801 (+MK-801), with 10 nM BPA and 20 μM CNQX (+CNQX), with 10 nM BPA and 1 μM nicardipine (+NIC), a 2 h treatment with 10 nM BPA in ACSF containing no Ca^{2+} (Ca^{2+} free), and 2 h washout with ACSF after 2 h treatment with 10 nM BPA (Washout). Note that the spine density did not change over 2–4 h incubations in ACFS. Therefore, the controls for the washout condition (incubated for 4 h) were not shown. Vertical axis shows the total number of spines per 1 μm dendritic segment. Results are means ± SEM. C*, $P < 0.05$ and C**, $P < 0.01$ vs. control (0 nM BPA); B**, $P < 0.01$ vs. 10 nM BPA. For each condition, we investigated 3–4 rats, 6–8 slices, 12–16 neurons, 24–32 dendrites and 1200–2000 spines.

4.1. Comparison of BPA and E2 effects on spinogenesis in slices

The elevation of BPA level to 10 nM (from less than 0.5 nM in acute slices) induced a rapid increase in the density of spines. The enhancing effect on spinogenesis was not greater at higher concentrations of BPA (100 nM) than those at lower concentrations of BPA (10 nM) (Fig. 1). BPA predominantly increased the density of middle-head spines by approx. 1.5-fold (Fig. 3). The reason is not clear for this selective increase, since BPA would affect all spines. We cannot eliminate the possibility that BPA may increase small-head spines then enlarge them to middle-head spines. Although receptors are different, some similarity is observed between BPA and E2 about modulation effects on spinogenesis in adult slices. The increase of middle-head spines also occurs upon 1 nM E2 treatments for 2 h in CA1 of hippocampus (Mukai et al., 2007). The E2-induced spinogenesis is also driven by Erk MAP kinase pathway (Mukai et al., 2007). Blocking of NMDA receptors by MK-801 abolishes the enhancing effects by E2 and BPA, suggesting that both E2 and BPA signaling need a basal level of Ca^{2+} which is kept by Ca^{2+} influx into spines via NMDA receptors due to spontaneous spiking (Ishii et al., 2007; Ogiue-Ikeda et al., 2008). As an another example, in organotypic hippocampal slice cultures, the pretreatment for 24 h with E2 or BPA at 10 nM exacerbates the CA3 neuronal damage caused by glutamate, due to enhanced spinogenesis by E2 or BPA (Sato et al., 2002).

4.2. ERRγ is a high affinity receptor for BPA

Although ERα had been assumed to be a receptor of BPA in earlier studies, the binding affinity of BPA to ERα is much lower (approx. 1/100–1/2000) than that of E2 (Kuiper et al., 1997; Morohoshi et al., 2005). Therefore, nanomolar BPA probably cannot induce significant effects on spinogenesis through ERα. On the other hand, BPA tightly binds to ERRγ (Takayanagi et al., 2006). To identify the receptor responsible for the BPA-induced modulation of spinogenesis, we used OH-Tam, an antagonist of ERRγ/ERα/ERβ (Fitts et al., 2011), and ICI, an antagonist of ERα/ERβ. OH-Tam completely suppressed the enhancement of spinogenesis by BPA, however, ICI did not suppress the BPA-induced enhancement of spinogenesis. Therefore, we conclude that ERRγ is a high affinity functional receptor for BPA. Note that E2 does not bind to ERRγ (Takayanagi et al., 2006).

BPA rapidly activates the transcription factor, cAMP-responsive element binding protein (CREB) in pancreatic β-cells (Quesada et al., 2002). Phosphorylated CREB is rapidly (~5 min) increased after application of 1 nM of BPA. The increase in phosphorylated CREB is not inhibited by ICI, implying that ERα/ERβ is not involved in these processes.

Until the current study, ERRγ has not been proven as a functional BPA receptor, although ERRγ is shown as a tight binding site of BPA. By means of the luciferase reporter gene assay, ERRγ shows constitutive transcriptional activity even without any ligand, including BPA. OH-Tam inhibits this ERRγ transcriptional activity by binding strongly to ERRγ with IC_{50} of 10.9 nM (Coward et al., 2001). BPA also binds strongly to ERRγ with IC_{50} of 13 nM (Takayanagi et al., 2006). BPA antagonizes the deactivation activity of OH-Tam, resulting in the recovery of the transcriptional activity of ERRγ. In other words, OH-Tam is an inverse agonist. BPA alone, however, cannot modulate the high basal transcriptional activity of ERRγ (Takayanagi et al., 2006; Okada et al., 2008), preventing assignment of ERRγ as BPA receptor. Fortunately in the current study, we could demonstrate the function of ERRγ as an inducer of spinogenesis upon binding of BPA. It is, however, also possible to explain that an endogenous inverse agonist of ERRγ (if the inverse agonist exists) inhibits ERRγ in the absence of BPA, and that BPA application reverses this inhibition. This explanation assumes that synaptic ERRγ is also a constitutively active receptor protein, which is the case for nuclear ERRγ.

Although ERRγ is highly expressed in adult rat brain (Eudy et al., 1998; Heard et al., 2000; Lorke et al., 2000), localization of ERRγ in the hippocampus had not been fully demonstrated. We showed that ERRγ is significantly expressed in pyramidal neurons and granule cells in the hippocampus as judged from immunostaining and Western blot analysis (Fig. 4). Since ERRγ may phosphorylate CREB, nanomolar BPA could also alter gene expression. Further investigations are important to fully clarify the ERRγ-driving signaling in modulation of synaptic plasticity.

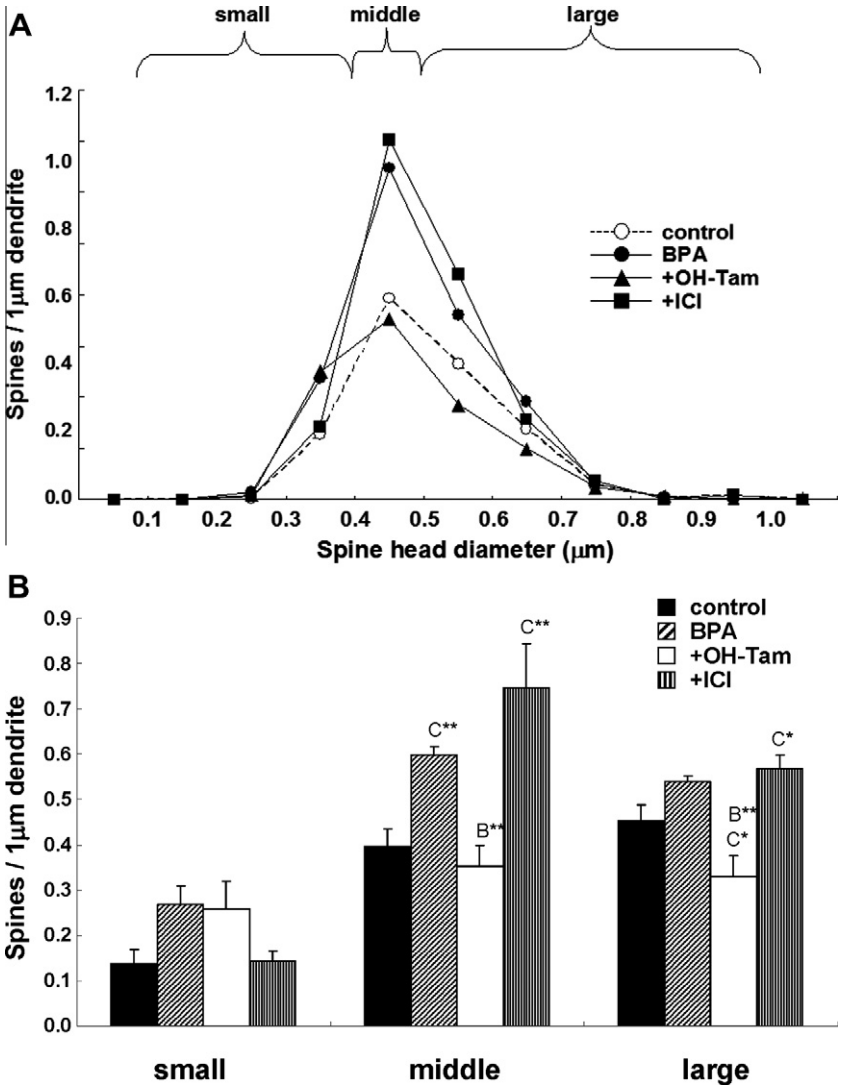

Fig. 3. Spine morphological analysis of CA1 neurons (A) Histogram of spine head diameter. Vertical axis is the average number of spines per 1 μm dendritic segment. A 2 h treatment without BPA (control, open circle), with 10 nM BPA (BPA, closed circle), with 10 nM BPA plus 1 μM OH-Tam (+OH-Tam, closed triangle), and with 10 nM BPA plus 1 μM ICI (+ICI, closed square). (B) Density of three subtypes of dendritic spines after a 2 h treatment without BPA (Control), with 10 nM BPA (BPA), with 10 nM BPA plus 1 μM OH-tam (+OH-Tam), and with 10 nM BPA plus 1 μM ICI (+ICI). In each subtype of spines, different treatment groups are indicated as: control (closed column), BPA (hatched column), +OH-Tam (open column), and +ICI (vertically striped column) from left to right. Results are reported as means ± SEM. C*, $P < 0.05$ and C**, $P < 0.01$ to control with 0 nM BPA; B**, $P < 0.01$ to 10 nM BPA. For each condition, we investigated 3–4 rats, 6–8 slices, 12–16 neurons, 24–32 dendrites and 1200–2000 spines.

4.3. In vivo effects of BPA

Electron microscopic investigations show *in vivo* rapid BPA effects (~30 min) on the spine-synapse density using ovariectomized (OVX) female adult rats (MacLusky et al., 2005). The s.c. injection of E2 (60 μg/kg) significantly increases/rescues the spine-synapse density in the hippocampus. Although application of BPA alone does not affect the spine-synapse density, co-application of BPA with E2 suppresses the E2-induced increase in the spine-synapse density. The rapid inhibitory effects of 0.1 nM BPA application on 0.1 nM E2-induced phosphorylation of MAP kinase are observed for cerebellar granule cells *in vivo* at postnatal 10 stage (Zsarnovszky et al., 2005). Interestingly, both BPA alone and E2 alone activate MAP kinase in cerebellar systems. An additional high-affinity BPA binding site is proposed in order to explain these BPA effects from these investigations. The current study implies that ERRγ can be this high-affinity BPA binding site.

These *in vivo* results should be explained depending on BPA and E2 actions in complex neural circuits. The anatomical neural circuits are very different between hippocampus *in vivo* and isolated slices. As shown in Fig. S3, hippocampus *in vivo* receives complicated projections of cholinergic neurons from Medial Septum/Diagonal Band of Broca (MSDB), serotonergic neurons from Median Raphe (MR), and glutamatergic neurons from supramammillary area (SUM). In addition GABAergic projections are present. These neurons express ERα or ERβ (Leranth et al., 2000). ERRγ is expressed in MSDB (Lorke et al., 2000), but ERRγ expression in MR region is not clear. These neurons project to GABA neurons and pyramidal neurons (PY) within the hippocampus. Therefore "BPA-induced suppressive modification of E2-induced enhanced spinogenesisis" consists of complicated processes, and is difficult to explain logically at the moment. We should consider many possible signaling pathways for explanation of these *in vivo* events. (Pathway 1) E2 activates cholinergic or serotonergic neurons → activates GABA neurons → suppresses PY. (Pathway 2) E2 activates cholinergic neurons → activates PY. (Pathway 3) BPA suppresses E2 action within cholinergic neurons (via ERRγ) → BPA and E2 act only in PY and GABA neurons. (Pathway 4) BPA does not

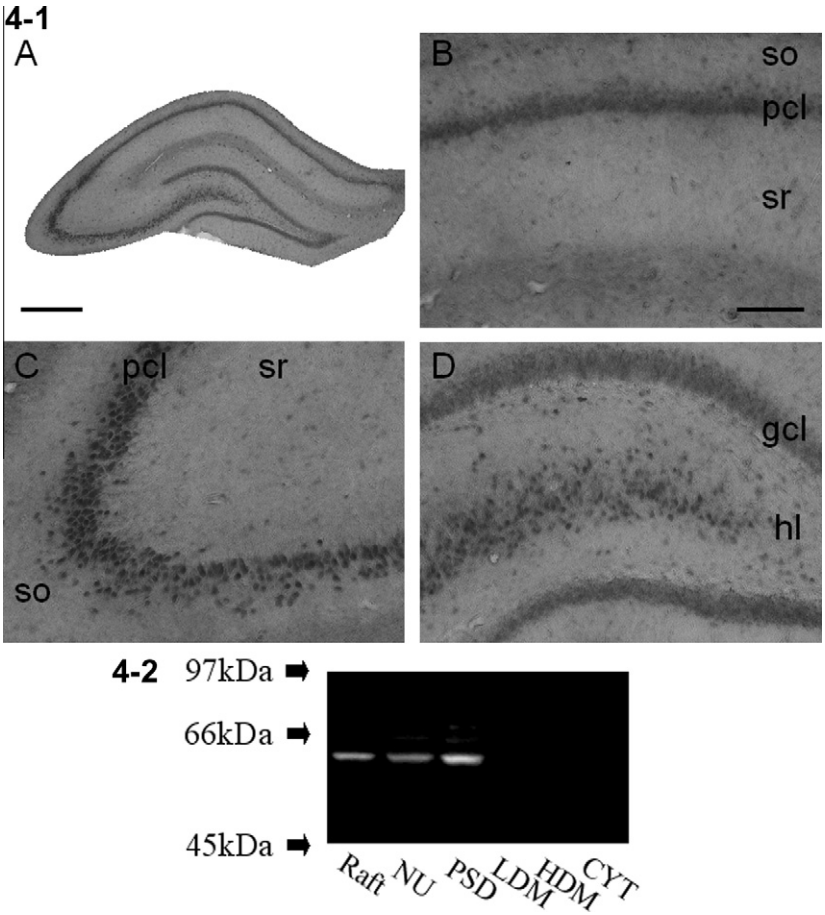

Fig. 4. ERRγ expression in the hippocampus (4-1) Immunohistochemical staining of ERRγ in hippocampal slices. (A) coronal section of the whole hippocampal formation; (B) CA1; (C) CA3; (D) DG. so, stratum oriens; pcl, pyramidal cell layer; sr, stratum radiatum; gcl, granule cell layer; hl, hilus. Scale bar, 500 μm for (A), and 200 μm for (B). (B)–(D) are with same magnification. (4-2) Western blot analysis of ERRγ in subcellular fractions of the hippocampus. From left to right, the dendritic raft fraction (Raft), nuclear fraction (NU), postsynaptic density fraction (PSD), low density membrane fraction (LDM), high density membrane fraction (HDM) and cytoplasmic fraction (CYT). LDM contains presynaptic fraction and HDM contains microsomal fraction. The amount of protein applied was 20 μg for each lane.

suppress E2 action in cholinergic neurons → E2 activates GABA neurons → suppresses PY. (Pathway 5) Direct BPA and E2 actions in intra-hippocampal GABA neurons. (Pathway 6) Direct BPA and E2 actions in PY. Other signaling pathways may also be present.

On the other hand, in our isolated hippocampal slices, we can focus on analysis of direct BPA effects on glutamatergic neurons and GABAergic neurons. In the current study, since ERRγ was expressed in entire PY whose population was much greater than that of GABAergic interneurons, the observed effect of BPA on hippocampal slices primarily caused by the BPA effect on PY.

It should be noted that BPA elevated the spine density of PY in isolated slices, however, BPA does not have any effect on the spine density of PY in hippocampus *in vivo*. These differences imply the clear difference of BPA action due to different neural circuits between slices and hippocampus *in vivo*.

We also should consider the difference between adult stage and developing stage. For example, in adult cerebellum, E2 only effects are localized to specific interneurons (ventrolateral portion of the soma and axon hillock of Purkinje cells), which is very different from E2 effects on entire granule cells at P10 developmental stage (Zsarnovszky et al., 2005). BPA effects in adult stage were not investigated, and therefore we do not know interactions between BPA and E2 in adult cerebellum.

Primary cultured neurons are also important to examine because of their simple structures without complicated neural circuits. In cultured hippocampal neurons, BPA rapidly increases the length of filopodia spines (Xu et al., 2010). E2 also increases the length of filopodia, however, BPA addition with E2 decreases the filopodia length to some extent.

4.4. Exposure to BPA in the human brain

Concerning endocrine organs, human BPA exposure (at μg/kg low dosage) might be insufficient to elicit significant responses, due to weak bioactivity in standard tests of estrogenicity, such as the rat uterotrophic assay (Ashby, 2001; Degen et al., 2002; EC Scientific Committee on Food, 2002; Japan Ministry of the Environment's ExTEND 2005; US Environmental Protection Agency, 1993). However, the brain may be sensitive to low dose BPA exposure in humans or animals, for example, BPA exposure (at 50 μg/kg low dosage) over a 28 day period inhibits the E2-induced remodeling of spine synapses in the ovariectomized monkey hippocampus (Leranth et al., 2008). Possible risks of low dose exposure to BPA are warned, for example, in behavior of children (Braun et al., 2011; US National Toxicology Program, 2008; Canadian Ministry of Health and Environment, 2008). Low dosage of μg/kg BPA may induce nanomolar plasma concentration of BPA. The BPA concentrations in male human plasma and male rat plasma are approx. 1.5 ng/ml (6.5 nM) and 24.9 ng/ml (109 nM), respectively (Takeuchi and Tsutsumi, 2002; Takeuchi et al., 2004). The plasma BPA may reach the brain and be accumulated without detoxification, as judged from no significant conversion of ^{3}H-BPA to other metabolites in hippocampal slices over 5 h (HPLC analysis, data not shown). These results are consistent with a significant level of

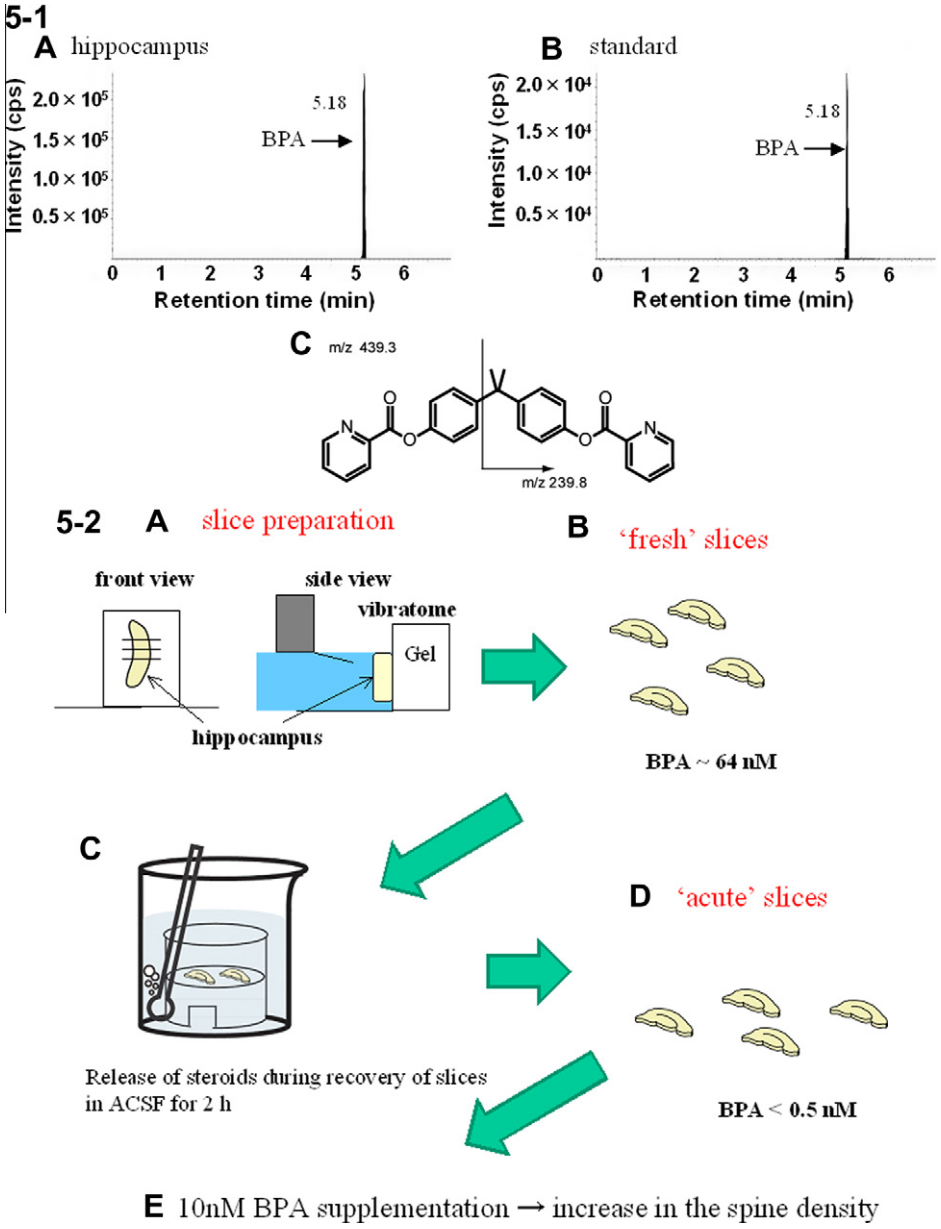

Fig. 5. Mass-spectrometric analysis of hippocampal BPA. (5-1) LC–MS/MS ion chromatogram of BPA from 'fresh' hippocampal slices before incubation with ACSF. Shaded portion indicates the fragmented ion of BPA-dipicolinoyl-ester (m/z 239.8) extracted from 'fresh' hippocampal slices (A) or standard BPA-dipicolinoyl-ester (B). Both fragmented ions have the same retention time, t = 5.18 min. The vertical axis indicates the intensity of the fragmented ions of BPA-dipicolinoyl-ester. The time at the injection to LC system was defined as t = 0. (C) Structures of BPA-dipicolinoyl-ester (m/z 439.3) and its fragmented ion used for analysis with LC–MS/MS. Both BPA-dipicolinoyl-ester and its fragmented ion have a single charge by induced-inonization. (5-2) Decrease of BPA level in 'acute' slices by recovery incubation (A) Hippocampal slices are prepared with a vibratome. (B) 'Fresh' slices contain a high level of BPA (~64 nM). (C) During recovery incubation of slices in steroid-free ACSF for 2 h, steroids are released to outer medium. (D) 'Acute' hippocampal slices have very low level of BPA < 0.5 nM. (E) 10 nM BPA supplementation can increase the spine density.

BPA (~64 nM) accumulated in the hippocampus of adult male rats (Fig. 5).

Taken together, we emphasize that even nanomolar low dosage of BPA could induce significant effects on synaptic plasticity of the hippocampus in mammals.

Acknowledgments

We thank Prof. J.A. Rose (Ritsumeikan University) and Dr. Anna Barron (Univ. of Tokyo) for critical reading of the manuscript. Drs. S. Homma and M. Okuyama (Aska Pharma Medical) are acknowledged for technical assistance of mass-spectrometric analysis.

Appendix A. Supplementary data

Supplementary data associated with this article can be found, in the online version, at doi:10.1016/j.mce.2012.01.008.

References

Al-Hiyasat, A.S., Darmani, H., Elbetieha, A.M., 2002. Effects of bisphenol A on adult male mouse fertility. Eur. J. Oral Sci. 110, 163–167.
Ashby, J., 2001. Increasing the sensitivity of the rodent uterotrophic assay to estrogens, with particular reference to bisphenol A. Environ. Health Perspect. 109, 1091–1094.
Braun, J.M., Kalkbrenner, A.E., Calafat, A.M., Yolton, K., Ye, X., Dietrich, K.N., Lanphear, B.P., 2011. Impact of early-life bisphenol A exposure on behavior and executive function in children. Pediatrics 128, 873–882.

Canadian Ministry of Health and Environment, 2008. Health Risk Assessment of Bisphenol A from Food Packaging Applications. Available from: <http://www.hc-sc.gc.ca/fn-an/securit/packag-emball/bpa/bpa_hra-ers-eng.php>.

Carr, R., Bertasi, F., Betancourt, A., Bowers, S., Gandy, B.S., Ryan, P., Willard, S., 2003. Effect of neonatal rat bisphenol A exposure on performance in the Morris water maze. J. Toxicol. Environ. Health A 66, 2077–2088.

Chinta, S.J., Kommaddi, R.P., Turman, C.M., Strobel, H.W., Ravindranath, V., 2005. Constitutive expression and localization of cytochrome P-450 1A1 in rat and human brain: presence of a splice variant form in human brain. J. Neurochem. 93, 724–736.

Cohen, R.S., Blomberg, F., Berzins, K., Siekevitz, P., 1977. The structure of postsynaptic densities isolated from dog cerebral cortex. I. Overall morphology and protein composition. J. Cell Biol. 74, 181–203.

Coward, P., Lee, D., Hull, M.V., Lehmann, J.M., 2001. 4-Hydroxytamoxifen binds to and deactivates the estrogen-related receptor gamma. Proc. Natl. Acad. Sci. USA 98, 8880–8884.

Degen, G.H., Janning, P., Wittsiepe, J., Upmeier, A., Bolt, H.M., 2002. Integration of mechanistic data in the toxicological evaluation of endocrine modulators. Toxicol. Lett. 127, 225–237.

Duan, H., Wearne, S.L., Morrison, J.H., Hof, P.R., 2002. Quantitative analysis of the dendritic morphology of corticocortical projection neurons in the macaque monkey association cortex. Neuroscience 114, 349–359.

EC Scientific Committee on Food, 2002. Opinion of the scientific committee on food on bisphenol A. Brussels:European Commission Health & Consumer Protection Directorate- General. Available from: <http://ec.europa.eu/food/fs/sc/scf/out128_en.pdf>.

Eudy, J.D., Yao, S., Weston, M.D., Ma-Edmonds, M., Talmadge, C.B., Cheng, J.J., Kimberling, W.J., Sumegi, J., 1998. Isolation of a gene encoding a novel member of the nuclear receptor superfamily from the critical region of Usher syndrome type IIa at 1q41. Genomics 50, 382–384.

Fisher, J.S., Turner, K.J., Brown, D., Sharpe, R.M., 1999. Effect of neonatal exposure to estrogenic compounds on development of the excurrent ducts of the rat testis through puberty to adulthood. Environ. Health Perspect. 107, 397–405.

Fitts, J.M., Klein, R.M., Powers, C.A., 2011. Tamoxifen regulation of bone growth and endocrine function in the ovariectomized rat: discrimination of responses involving estrogen receptor alpha/estrogen receptor beta, G protein-coupled estrogen receptor, or estrogen-related receptor gamma using fulvestrant (ICI 182780). J. Pharmacol. Exp. Ther. 338, 246–254.

Fujimoto, T., Kubo, K., Aou, S., 2006. Prenatal exposure to bisphenol A impairs sexual differentiation of exploratory behavior and increases depression-like behavior in rats. Brain Res. 1068, 49–55.

Grote, K., Stahlschmidt, B., Talsness, C.E., Gericke, C., Appel, K.E., Chahoud, I., 2004. Effects of organotin compounds on pubertal male rats. Toxicology 202, 145–158.

Hajszan, T., Leranth, C., 2010. Bisphenol A interferes with synaptic remodeling. Front Neuroendocrinol. 31, 519–530.

Halldin, K., Axelsson, J., Brunstrom, B., 2005. Effects of endocrine modulators on sexual differentiation and reproductive function in male Japanese quail. Brain Res. Bull. 65, 211–218.

Heard, D.J., Norby, P.L., Holloway, J., Vissing, H., 2000. Human ERRgamma, a third member of the estrogen receptor-related receptor (ERR) subfamily of orphan nuclear receptors: tissue-specific isoforms are expressed during development and in the adult. Mol. Endocrinol. 14, 382–392.

Hojo, Y., Higo, S., Ishii, H., Ooishi, Y., Mukai, H., Murakami, G., Kominami, T., Kimoto, T., Honma, S., Poirier, D., Kawato, S., 2009. Comparison between hippocampus-synthesized and circulation-derived sex steroids in the hippocampus. Endocrinology 150, 5106–5112.

Ishii, H., Tsurugizawa, T., Ogiue-Ikeda, M., Asashima, M., Mukai, H., Murakami, G., Hojo, Y., Kimoto, T., Kawato, S., 2007. Local production of sex hormones and their modulation of hippocampal synaptic plasticity. Neuroscientist 13, 323–334.

Japan Ministry of the Environment's ExTEND, 2005. Summary of Public Opinions and MOE's Views on Perspectives on Endocrine Disrupting Effects of Substances. Available from: <http://www.env.go.jp/en/chemi/ed.html>.

Kawato, S., Hojo, Y., Kimoto, T., 2002. Histological and metabolism analysis of P450 expression in the brain. Methods Enzymol. 357, 241–249.

Kimoto, T., Tsurugizawa, T., Ohta, Y., Makino, J., Tamura, H., Hojo, Y., Takata, N., Kawato, S., 2001. Neurosteroid synthesis by cytochrome p450-containing systems localized in the rat brain hippocampal neurons: *N*-methyl-D-aspartate and calcium-dependent synthesis. Endocrinology 142, 3578–3589.

Kishimoto, W., Hiroi, T., Shiraishi, M., Osada, M., Imaoka, S., Kominami, S., Igarashi, T., Funae, Y., 2004. Cytochrome P450 2D catalyze steroid 21-hydroxylation in the brain. Endocrinology 145, 699–705.

Kubo, K., Arai, O., Omura, M., Watanabe, R., Ogata, R., Aou, S., 2003. Low dose effects of bisphenol A on sexual differentiation of the brain and behavior in rats. Neurosci. Res. 45, 345–356.

Kuiper, G.G., Carlsson, B., Grandien, K., Enmark, E., Haggblad, J., Nilsson, S., Gustafsson, J.A., 1997. Comparison of the ligand binding specificity and transcript tissue distribution of estrogen receptors alpha and beta. Endocrinology 138, 863–870.

Leranth, C., Shanabrough, M., Horvath, T.L., 2000. Hormonal regulation of hippocampal spine synapse density involves subcortical mediation. Neuroscience 101, 349–356.

Leranth, C., Hajszan, T., Szigeti-Buck, K., Bober, J., MacLusky, N.J., 2008. Bisphenol A prevents the synaptogenic response to estradiol in hippocampus and prefrontal cortex of ovariectomized nonhuman primates. Proc. Natl. Acad. Sci. USA 105, 14187–14191.

Lorke, D.E., Susens, U., Borgmeyer, U., Hermans-Borgmeyer, I., 2000. Differential expression of the estrogen receptor-related receptor gamma in the mouse brain. Brain Res. Mol. Brain Res. 77, 277–280.

MacLusky, N.J., Hajszan, T., Leranth, C., 2005. The environmental estrogen bisphenol A inhibits estradiol-induced hippocampal synaptogenesis. Environ. Health Perspect. 113, 675–679.

Miksys, S.L., Tyndale, R.F., 2002. Drug-metabolizing cytochrome P450s in the brain. J. Psychiatry Neurosci. 27, 406–415.

Morohoshi, K., Yamamoto, H., Kamata, R., Shiraishi, F., Koda, T., Morita, M., 2005. Estrogenic activity of 37 components of commercial sunscreen lotions evaluated by in vitro assays. Toxicol. In Vitro 19, 457–469.

Mukai, H., Tsurugizawa, T., Murakami, G., Kominami, S., Ishii, H., Ogiue-Ikeda, M., Takata, N., Tanabe, N., Furukawa, A., Hojo, Y., Ooishi, Y., Morrison, J.H., Janssen, W.G., Rose, J.A., Chambon, P., Kato, S., Izumi, S., Yamazaki, T., Kimoto, T., Kawato, S., 2007. Rapid modulation of long-term depression and spinogenesis via synaptic estrogen receptors in hippocampal principal neurons. J. Neurochem. 100, 950–967.

Mukai, H., Hatanaka, Y., Mitsuhashi, K., Hojo, Y., Komatsuzaki, Y., Sato, R., Murakami, G., Kimoto, T., Kawato, S., 2011. Automated analysis of spines from confocal laser microscopy images: application to the discrimination of androgen and estrogen effects on spinogenesis. Cereb. Cortex 21, 2704–2711.

Ogiue-Ikeda, M., Tanabe, N., Mukai, H., Hojo, Y., Murakami, G., Tsurugizawa, T., Takata, N., Kimoto, T., Kawato, S., 2008. Rapid modulation of synaptic plasticity by estrogens as well as endocrine disrupters in hippocampal neurons. Brain Res. Rev. 57, 363–375.

Okada, H., Tokunaga, T., Liu, X., Takayanagi, S., Matsushima, A., Shimohigashi, Y., 2008. Direct evidence revealing structural elements essential for the high binding ability of bisphenol A to human estrogen-related receptor-gamma. Environ. Health Perspect. 116, 32–38.

Quesada, I., Fuentes, E., Viso-Leon, M.C., Soria, B., Ripoll, C., Nadal, A., 2002. Low doses of the endocrine disruptor bisphenol-A and the native hormone 17beta-estradiol rapidly activate transcription factor CREB. FASEB J. 16, 1671–1673.

Sato, K., Matsuki, N., Ohno, Y., Nakazawa, K., 2002. Effects of 17beta-estradiol and xenoestrogens on the neuronal survival in an organotypic hippocampal culture. Neuroendocrinology 76, 223–234.

Shinohara, Y., Hirase, H., Watanabe, M., Itakura, M., Takahashi, M., Shigemoto, R., 2008. Left-right asymmetry of the hippocampal synapses with differential subunit allocation of glutamate receptors. Proc. Natl. Acad. Sci. USA 105, 19498–19503.

Sorra, K.E., Harris, K.M., 2000. Overview on the structure, composition, function, development, and plasticity of hippocampal dendritic spines. Hippocampus 10, 501–511.

Takayanagi, S., Tokunaga, T., Liu, X., Okada, H., Matsushima, A., Shimohigashi, Y., 2006. Endocrine disruptor bisphenol A strongly binds to human estrogen-related receptor gamma (ERRgamma) with high constitutive activity. Toxicol. Lett. 167, 95–105.

Takeuchi, T., Tsutsumi, O., 2002. Serum bisphenol A concentrations showed gender differences, possibly linked to androgen levels. Biochem. Biophys. Res. Commun. 291, 76–78.

Takeuchi, T., Tsutsumi, O., Nakamura, N., Ikezuki, Y., Takai, Y., Yano, T., Taketani, Y., 2004. Gender difference in serum bisphenol A levels may be caused by liver UDP-glucuronosyltransferase activity in rats. Biochem. Biophys. Res. Commun. 325, 549–554.

Tokunaga, T., Liu, X., Okada, H., Matsushima, A., Nose, T., Shimohigashi, M., Shimohigashi, Y., 2006. Conformation change of α-helix peptide for sensing of deactivation of nuclear receptor: immunoassay using polyclonal antibody specific for the C-terminal α-Helix 12 of estrogen-related receptor γ (ERRγ). Peptide Sci. 176.

U.S. EPA, 1993, Bisphenol A, CASRN 80-05-7. Washington, DC:Integrated Risk Information System, U.S. Environmental Protection Agency. Available from: <http://www.epa.gov/iris/subst/0356.htm>.

US National Toxicology Program, 2008. NTP-CERHR Monograph on the Potential Human Reproductive and Developmental Effects of Bisphenol A. Available from: <http://ntp.niehs.nih.gov/ntp/ohat/bisphenol/bisphenol.pdf>.

Xu, X., Ye, Y., Li, T., Chen, L., Tian, D., Luo, Q., Lu, M., 2010. Bisphenol-A rapidly promotes dynamic changes in hippocampal dendritic morphology through estrogen receptor-mediated pathway by concomitant phosphorylation of NMDA receptor subunit NR2B. Toxicol. Appl. Pharmacol. 249, 188–196.

Zsarnovszky, A., Le, H.H., Wang, H.S., Belcher, S.M., 2005. Ontogeny of rapid estrogen-mediated extracellular signal-regulated kinase signaling in the rat cerebellar cortex: potent nongenomic agonist and endocrine disrupting activity of the xenoestrogen bisphenol A. Endocrinology 146, 5388–5396.

Supplementary material

Methods

Chemical synthesis of ERRγ C-terminal peptides

The C-terminal peptide fragment (residues 419-435) of ERRγ (GKVPMHKLFLEMLEAKV) was synthesized (0.1 mmol scale) on an automated peptide synthesizer ABI 433A (Applied Biosystems Inc., Foster City, CA, USA) using Rink Amide MBHA resin (Novabiochem, La Jolla, CA, USA) with Fmoc synthetic strategy. The synthetic peptide was liberated from the resin by Reagent K at 25˚C for 2 h. After evaporation, the residue was solidified with diethyl ether. Purification was carried out first by a gel filtration column (1.0 x 75 cm) of Sephadex G-15 (Amersham Bioscience, Piscataway, NJ, USA) eluted with 30% acetic acid. For further purification, reversed-phase high performance liquid chromatography (RP-HPLC) was performed on a preparative column (25 x 250 mm, Cica-Merck LiChrospher RP-18 (e), 5 mm) with a linear gradient of 0.1% trifluoroacetic acid and 80% acetonitrile and the fraction containing a pure peptide was pooled and lyophilized to obtain the final peptide sample.

The purity was verified by analytical RP-HPLC (4 x 250 mm, Cica-Merck LiChrospher 100 RP-18, 5 mm). Mass spectra were measured on a mass spectrometer Voyager^{TM} DE-PRO (PreSeptive Biosystems Inc., Framingham, MA, USA) by matrix-assisted laser desorption ionization time-of-flight (MALDI-TOF) to confirm the chemical structure of the peptide synthesized. To prepare an antibody against ERRγ C-terminal peptide, the thiol-containing amino acid Cys was attached to the N-terminus.

Preparation of polyclonal antibody

Synthesized Cys-attached ERRγ C-terminal peptide was chemically conjugated to a carrier protein keyhole limpet hemocyanin (KLH: Sigma-Aldrich). The cross-linking coupling between peptide and protein was performed with the heterobifunctional reagent *m*-maleimidobenzoyl-*N*-hydroxysuccinimide ester (MBS) (Pierce, Rockford, IL, USA), which contains *N*-hydroxysuccinimide ester and maleimide groups that allow covalent conjugation between the KLH amine and the PDF Cys-thiol groups. A polyclonal antibody was prepared by immunizing New Zealand

white rabbits with the KLH-conjugated ERRγ C-terminal peptide. After the final boost, blood was collected from the ear artery of rabbits for serum preparations. The serum was treated with KLH (0.5 mg/ml) overnight at 4˚C, and then the mixture was centrifuged (14,000 *g*) for 5 min. Purification by immunoprecipitation was repeated several times, and the supernatant collected was purified by affinity chromatography on a column packed with the gel of ERRγ C-terminal peptide-linked agarose (SulfoLink® Coupling Gel, Pierce).

Characterization of polyclonal antibody

ERRγ C-terminal peptide was conjugated to a carrier protein bovine thyroglobulin G (bThG). The cross-linking coupling was carried out by MBS, as for KLH-conjugated ERRγ C-terminal peptide. To examine the anti-ERRγ C-terminal peptide (merely denoted as anti-ERRγ pAb hereafter) by ELISA, the bThG-conjugated antigen peptide solutions were incubated for 2 h at 25˚C to immobilize them in the 96-well ELISA plate. HRP-conjugated anti-rabbit IgG (Jackson ImmunoResearch, West Grove, PA, USA) was used for the coloring at 405 nm on a microplate reader (Immuno-mini NJ-2300, Intermed, Tokyo). Prepared anti-ERRγ pAb was found to recognize very well the antigen peptide *per se*. However, this antibody did not react with the peptides derived from the C-terminal moieties of ERα and ERβ. Similar results were obtained also for ERRγ, ERα, and ERβ ligand-binding domain (LBD) proteins. Anti-ERRγ pAb reacted with ERRγ, but not with ERα and ERβ.

For the specific detection of ERRγ protein by anti-ERRγ pAb, the western blotting assay was also performed. For this identification, we tested GST-fused ERRγ-LBD together with GST-ERα-LBD and GST-ERβ-LBD. After electrophoresis, gels were electro-blotted onto Hybond-P (GE Healthcare; Chicago, IL, USA), and the blot was incubated for 2 h in the blocking solution (3% BSA-PBS with 0.1% Tween 20). After consecutive washings with PBST, the blot was further incubated for overnight in the presence of anti-ERRγ pAb. Visualization of proteins was performed by chemi-luminescence (GE Healthcare, Waukesha, WI, USA) using anti-mouse IgG horseradish peroxidase-conjugated secondary antibody. Again, anti-ERRγ pAb reacted with ERRγ, but not with ERα and ERβ (see Fig. S1).

Figures

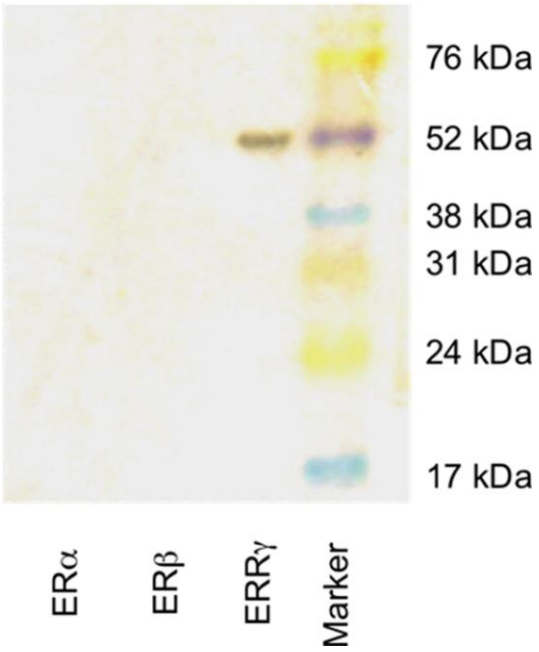

Figure S1

Western blotting analysis of GST-fused ERRγ-LBD, ERα-LBD and ERβ-LBD. Only ERRγ derivative (approx. 55 kDa) was detected by the polyclonal antibody anti-ERRγ pAb, and no cross-reactivity was observed for both ERα and ERβ derivatives.

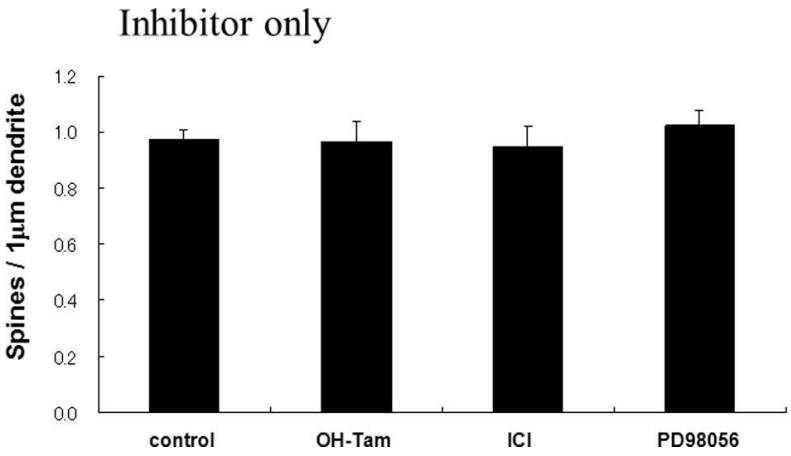

Figure S2

No effect of receptor antagonists and kinase inhibitor alone on the total spine density in CA1 neurons. Vertical axis shows the total number of spines per 1 μm dendritic segment. A 2 h treatment in ACSF without BPA

(0 nM BPA), with 1 μM OH-Tam (OH-Tam), with 1 μM ICI (ICI) and with 50 μM PD98059 (PD98059).

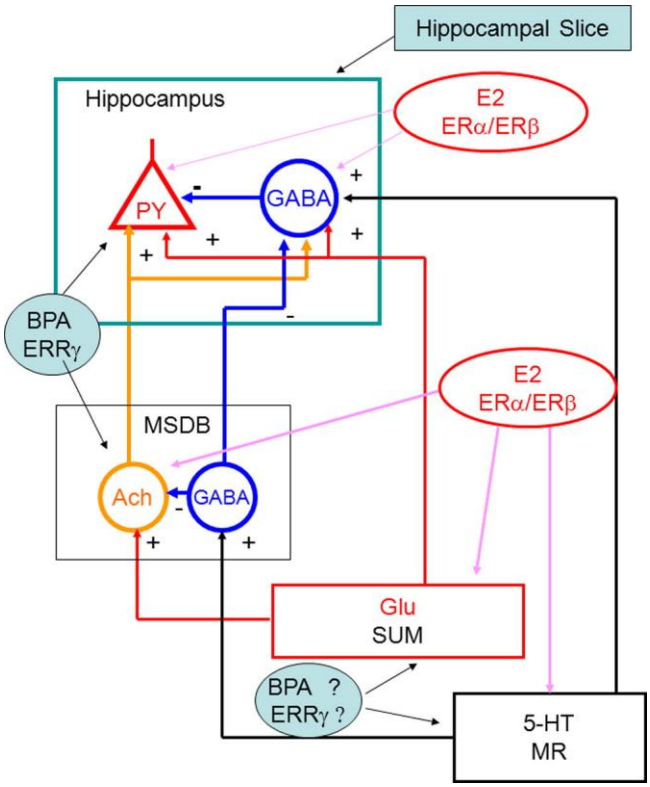

Figure S3

Neural circuits *in vivo* including the hippocampus. The hippocampus receives complex projections, including cholinergic neurons from medial septum and diagonal band of Broca (MSDB), serotonergic neurons from median raphe (MR), and glutamatergic neurons from supramammillary neucleus (SUM). GABAergic neurons are also included. ERα/ERβ is expressed in these neurons. Cholinergic neurons in MSDB express ERRγ. Isolated hippocampal slice has only local neural circuit.

Table S1

The intra- and inter-assay of accuracy and precision as well as the limit of quantification (LOQ) for BPA in mass-spectrometric analysis

	Intraassay		Interassay		LOQ
	Accuracy(%)	RSD(%)[a]	Accuracy(%)	RSD(%)	(pg/0.1g)[b]
BPA	102.8	4.7	98.9	3.6	5

Blank samples, prepared alongside hippocampal samples through the whole extraction and purification procedures, were spiked with BPA at 1, 5,10, 20 and 100 pg, and contents were determined by LC-MS/MS. Accuracy was expressed as a percentage of an analytical recovery rate of measured steroid content against spike amount. Results shown only for 5 pg for BPA.

[a]relative standard deviation.

[b]LOQ is expressed as pg/0.1 g. Because the average weight of one whole adult hippocampus (0.14 g) was close to 0.1 g, these LOQ values indicate the limit of quantification of steroids from nearly one hippocampus.